3-6-2008

Fabrication of nanostructures with high electrical conductivity on silicon surfaces using a laser-assisted scanning tunneling microscope

Kaijun Yi
University of Nebraska-Lincoln, kjyi1@bigred.unl.edu

Z. Y. Yang
University of Nebraska-Lincoln

Yongfeng Lu
University of Nebraska-Lincoln, ylu2@unl.edu

Fabrication of nanostructures with high electrical conductivity on silicon surfaces using a laser-assisted scanning tunneling microscope

K. J. Yi,[1] Z. Y. Yang,[1] and Y. F. Lu[1,a)]
[1]*Department of Electrical Engineering, University of Nebraska-Lincoln, Lincoln, Nebraska 68588-0511, USA*

(Received 23 July 2007; accepted 5 January 2008; published online 6 March 2008)

Nanostructures with high electrical conductivity were fabricated on silicon surfaces using a laser-assisted scanning tunneling microscope (LA-STM). The nanostructures, dots and lines, were fabricated on H-passivated *p*-doped silicon (110) surfaces. By precisely controlling the experimental conditions such as pulse energy and tip-surface gap distance, feature sizes (dot diameters and line widths) and heights of the fabricated nanostructures could be controlled. For instance, a dot with a diameter of 30 nm and a line with a width of 30 nm were obtained. In addition, scanning tunneling microscopy investigation of the structures revealed that their band gaps were changed during the LA-STM process. As a consequence, the local conductivity (more precisely the tunneling probability) was enhanced. Numerical simulations based upon the finite-difference-time-domain algorithm provide detailed insight into the spatial distribution of the enhanced optical field underneath the STM tip and associated physical phenomena. Potential applications of the developed nanostructuring process are anticipated in various nanotechnology fields, particularly in the field of nanoelectronics. © *2008 American Institute of Physics*. [DOI: 10.1063/1.2890422]

I. INTRODUCTION

The past decade has seen an unprecedented rapid growth of nanoscience research and engineering. Modern manufacturing industries, particularly for the fabrication of integrated circuit at nanoscales (i.e., nanoelectronics), demands innovative approaches to fabricate nanostructures, which are critical parts of quantum-effect devices for future highly integrated circuit building blocks.[1] Scanning tunneling microscope (STM), traditionally as an indispensable tool for ultrahigh-resolution imaging of surface morphology/structures and measurement of surface electronic structures, has offered possibilities to locally manipulate and modify material surfaces in nanometric or even atomic scales by using various STM interactions as contact forces, electrical fields, and electron beam induced effects or even a combination of these interaction mechanisms.[2–8] Laser-assisted STM (LA-STM), in which external energy is injected into the tip-substrate gap with laser radiation, is an alternative approach to perform surface nanostructuring and atomic manipulation. It has several advantages over STM-only counterpart such as versatile material processing and correlated property characterization.[9–17] This technique, stemming from the tip-enhanced Raman spectroscopy, employs a focused laser radiation at the tip apex. A local intensity enhancement of optical radiation near the tip apex with the resolution much beyond the optical diffraction can be achieved. The field enhancement is mainly explained by a combination of classical electrostatic lightning rod and surface plasmon excitation effects.[18–21] Till now, nanostructures with low electrical conductivity, i.e., nanooxidization of silicon as an energy barrier, have been intensively investigated using LA-STM. In contrast, however, the fabrication of nanostructures with high electrical conductivity using this method has not been fully investigated. The application of LA-STM to surface nanostructuring which will ultimately be utilized in micro- or nanoelectronics industry involves the completely understanding their electronic properties, which can be characterized by scanning tunneling spectroscopy (STS).[22–25]

In this study, the fabrication of nanostructures with high electrical conductivity, on *p*-type H-passivated silicon (110) surfaces using LA-STM, was investigated. Nanostructures (dots and lines) were fabricated. Their surface morphologies were characterized *in situ* by STM, while their electronic properties were characterized by STS. The dependence of nanostructure geometries on laser energy and number of pulses was investigated. The tip-induced enhancement of optical fields, the driving force to the nanofabrication, was numerically simulated based upon the finite-difference-time-domain (FDTD) algorithm and Lorentz–Drude model using the OPTIWAVE™ software package.[26]

II. SIMULATION

Knowing the electrical field distribution underneath a tip apex provides a meaningful understanding for experimental investigations of LA-STM. It helps to identify the key parameters involved in the fabrication process. For the purpose, the numerical simulation was conducted based upon the Lorentz–Drude model and FDTD algorithm using the OPTIWAVE™ software.

A number of theoretical research efforts have been made to understand the effects of the tip shape on the optical enhancement. The optical response of a cone with a semisphere tip apex can significantly simplify the problem. At the same time, this model can approximately represent the geometry of the tungsten tips used in experiments. As illustrated in Fig.

a)Author to whom correspondence should be addressed. Tel.: 402-472-8323. Electronic mail: ylu2@unl.edu.

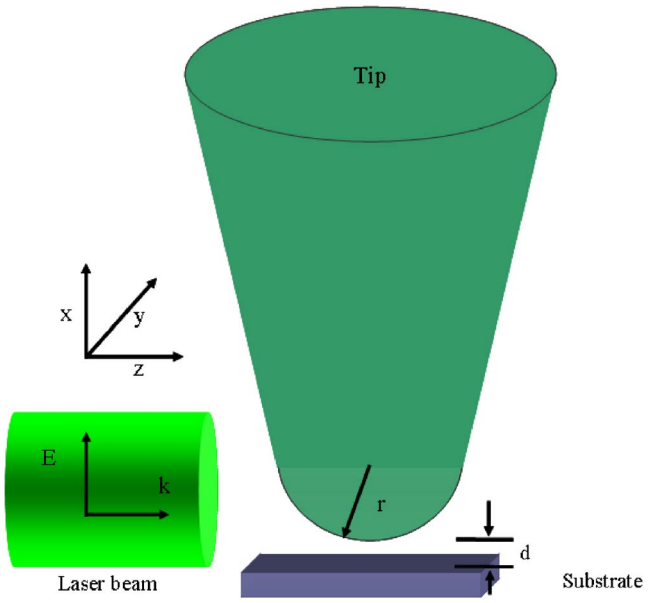

FIG. 1. (Color online) Representation of an STM tip under laser illumination used in the FDTD simulation.

1, a conical tungsten (W) tip is placed above a flat silicon surface. The tip-surface gap is illuminated by a Gaussian-shaped continuous plane wave propagating along the k direction (z axis). The main axis of the tip (x axis) is hence perpendicular to the k direction.

In modeling, a complex dielectric function, $\varepsilon_r(\omega)$, for the tungsten tip based upon the Lorentz–Drude model in frequency domain is given[27,28]

$$\varepsilon_r(\omega) = \varepsilon_{r,\infty} + \sum_{m=0}^{M} \frac{G_m \Omega_m^2}{\omega_m^2 - \omega^2 + j\omega\Gamma_m}. \quad (1)$$

Here, $\varepsilon_{r,\infty}$ is the relative permittivity in the infinity frequency, Ω_m is the plasma frequency, ω_m is the resonant frequency, and Γ_m is the damping factor or collision frequency.

Using the polarization principle in the Maxwell equations, the transformation of Eq. (1) from frequency domain to time domain can be expressed as

$$\mu_0 \frac{\partial \mathbf{H}}{\partial t} = \nabla \times \mathbf{E}, \quad (2)$$

$$\varepsilon_{r,\infty}\varepsilon_0 \frac{\partial \mathbf{E}}{\partial t} + \sum_{m=0}^{M} \frac{\partial \mathbf{P}_m}{\partial t} = -\nabla \times \mathbf{H}, \quad (3)$$

$$\frac{\partial \mathbf{P}_m}{\partial t^2} + \Gamma_m \frac{\partial \mathbf{P}_m}{\partial t} + \omega_m^2 \mathbf{P}_m = \varepsilon_0 G_m \Omega_m^2 \mathbf{E}. \quad (4)$$

Here, $\mathbf{P}_m$ is the dispersive polarization denoting the nonlinear polarization, G_m is related to the oscillation strengths, μ_0 is the permeability of vacuum, and ε_0 is the permittivity of free space. The FDTD algorithm is derived from the above equations.

The influences of the beam polarization, tip radius, and silicon substrate were investigated. Specifically, tips with radii (r) ranging from 15 to 50 nm were used to approximate the practical conditions. A typical tip-surface distance (d) was selected to be 1 nm. The electric field of the plane wave was assumed to be 1 V/m.

Figures 2(a) and 2(b) show the images of the electric field distribution around a tungsten tip of a 10 nm radius with the laser polarization in parallel with or perpendicular to the tip axis, respectively. The simulation results show that an electric field in parallel with the tip axis is required to achieve a strongly enhanced optical field underneath the tip apex, which is in agreement with the previous reports.[29,30] Lightning rod effects can be used to explain this enhancement phenomenon. The free electrons in the tip react to the external electromagnetic excitation by inducing surface charges. Due to the presence of a geometrical singularity, the local surface charge density is drastically increased in the near field of the tip apex, leading to a localized optical enhancement. In the following simulations, the laser polarization is kept in parallel with the tip axis.

Figures 3(a) and 3(b) show the images of the electric field distributions around a tip of a 25 nm radius with and without the presence of a silicon substrate. Figures 3(c) and 3(d) show the images of the electric field distributions around a tip of a 50 nm radius with and without the presence of a silicon substrate. It can be seen that the optical field is enhanced more strongly for the tip of a smaller radius. The enhanced optical fields are mostly constrained in an area of 1×1 nm^2. In addition, it can also be observed that the enhancement in the presence of a substrate is over two times stronger than the case in the absence of the substrate, indicating that the interplay between the substrate and the tip apex is significant.

III. EXPERIMENTAL DETAILS

The experimental steps include the preparation of H-passivated silicon substrates, fabrication of tungsten tips,

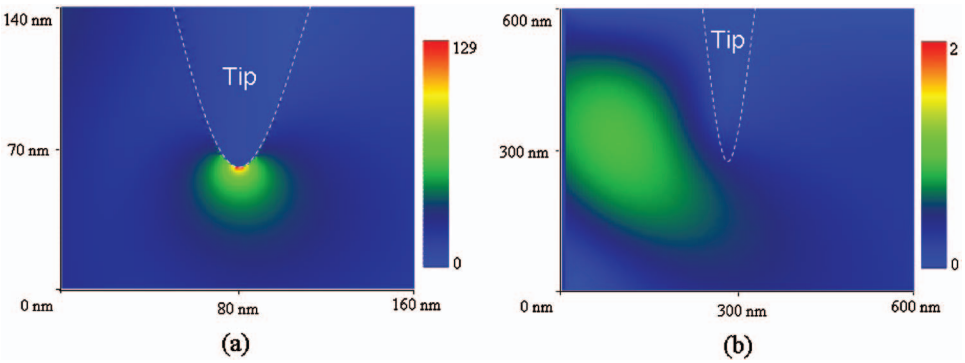

FIG. 2. (Color) Images of the electric field distribution near a tungsten tip with a 10 nm radius, irradiated by a laser beam with the polarization (a) in parallel with and (b) perpendicular to the tip axis.

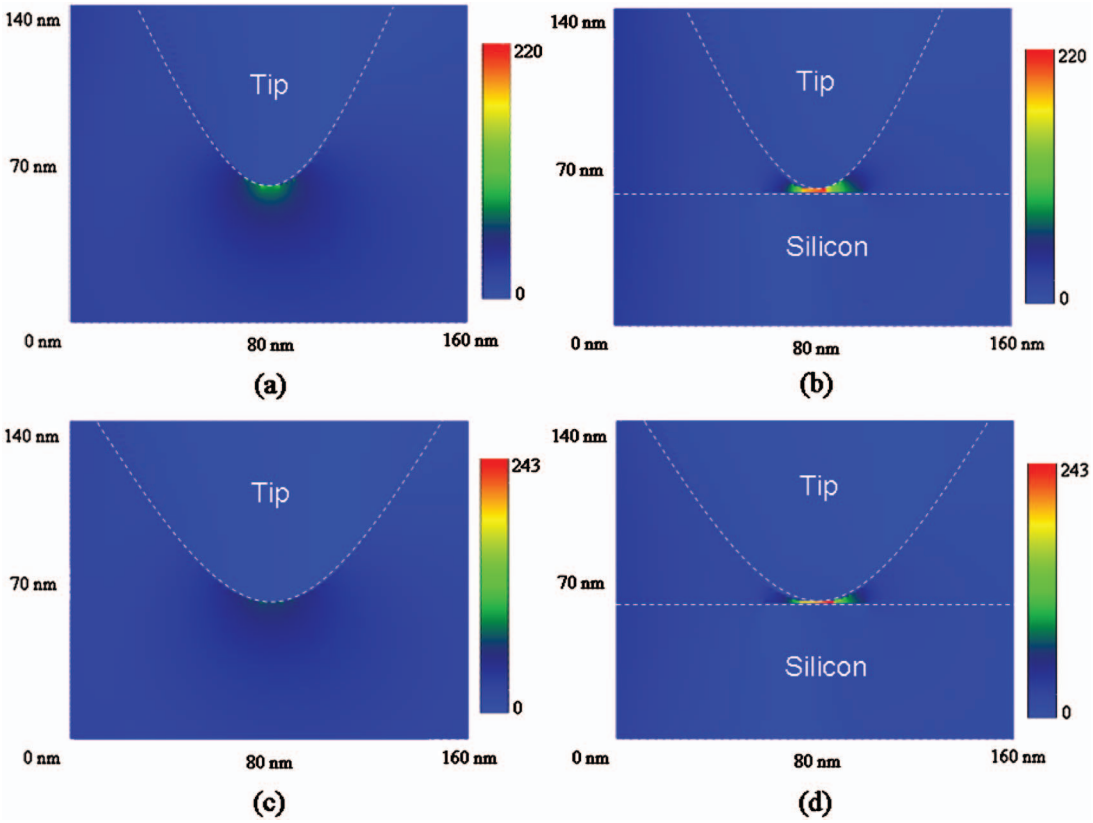

FIG. 3. (Color) Images of the electric field distribution around (a) a 25-nm-radius tip alone, (b) a 25-nm-radius tip in the presence of a silicon substrate, (c) a 50-nm-radius tip alone, and (d) a 50-nm-radius tip in the presence of a silicon substrate.

processing of nanostructures on the as-prepared silicon substrates, and characterization of the fabricated nanostructures.

P-type silicon (110) substrates (Virginia Semiconductor) with a resistivity of 0.02–0.09 Ω cm were cleaned by an ultrasonic cleaner with acetone and alcohol solutions for 10 min each, followed by a passivation process in 5% HF solution for 5 min. The substrates were then dried with a nitrogen gas. Subsequently, they were kept in an acetone-filled container to avoid surface oxidization.

Tungsten tips were fabricated from a W wire with a diameter of 0.25 mm by electrochemical (EC) etching system using a dc current. The tip geometries were characterized by a field-emission scanning electron microscope (SEM, Hitachi S-4700). Generally, the tips with different geometries could be prepared by tuning the position of the wire immersed in the electrolyte. However, due to the surface tension between the tip surface and the electrolyte, precise control over the length of tips is required.

The schematic diagram of the experimental setup for surface nanostructuring by LA-STM is shown in Fig. 4. The setup is composed of an STM (Agilent, PicoPlus 5), a *Q*-switched pulsed Nd-YAG (YAG denotes yttrium aluminum garnet) laser with a pulse width of 7 ns and a wavelength of 532 nm, and optics for delivering the laser beam. The STM can operate both in open loop and close loop modes by changing different scanners. An on-axis optical microscope equipped with a charge coupled device (CCD) camera provides zoom view of substrate surfaces for beam alignment on the tip apex. The focused laser beam is introduced to the tip-surface gap from the front side of the probe head.

Alignment of the laser beam was performed under the optical microscope by observing the diffraction light from the tip. To make sure that the nanostructure was induced only from the near-field effects of the tip, the incident laser beam was adjusted to be completely perpendicular to the tip axis or in parallel with the sample surface. The STM scanner was placed in a transparent environment chamber to effectively suppress environmental noises. To perform the nanofabrication, laser pulses were applied while the tip-surface distance was within the tunneling range. The incident laser beam was focused before reaching the tip-surface gap. The STM was kept in the constant-current mode with a tunneling current of 3 nA both for fabrication and imaging. The surface morphology was characterized *in situ* by turning off the laser. The STS was performed to measure the current-voltage (*I-V*) characteristics from which the differential conductance was derived.

IV. RESULTS AND DISCUSSION

The tip fabrication process is governed by a number of factors such as solution concentration, tip-electrode distance, and etching time. Typically, the tungsten tips have curvature radii varying from 10 to 50 nm. An image of a typical tip is shown in the top-right inset in Fig. 4. The length of the tip from the etching-starting point to the tip apex is about 200 μm, with a curvature radius of approximately 20 nm.

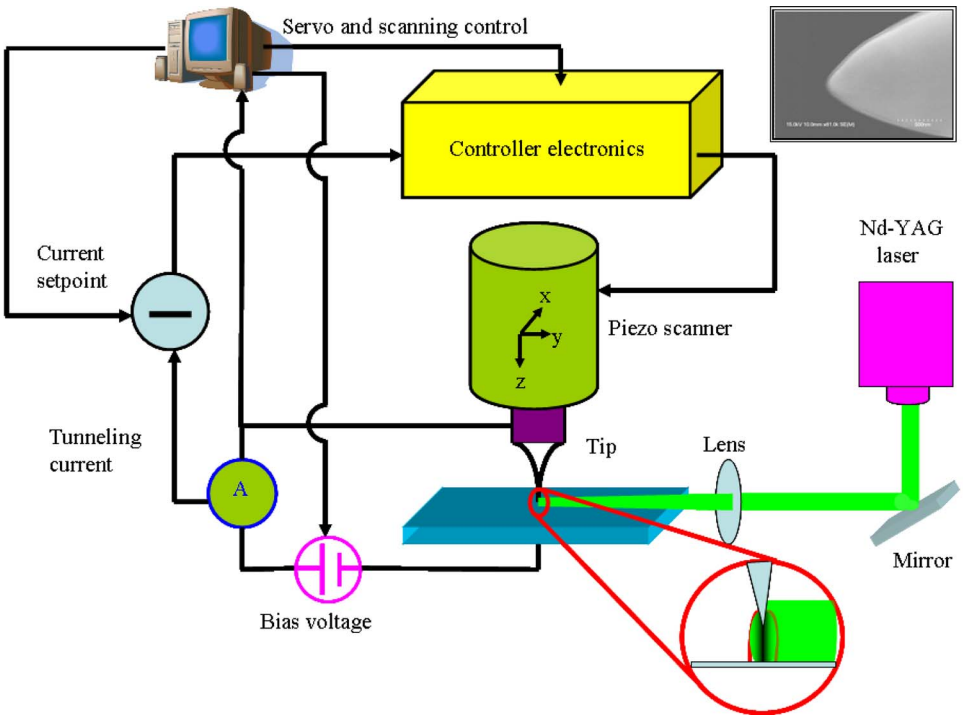

FIG. 4. (Color online) Experimental setup for surface nanostructuring by LA-STM. The top-right inset is the SEM image of a tip.

The tips with lengths longer than 300 μm are not suitable for LA-STM experiments because long tips become sensitive to noises and system vibrations. The curvature shape or aspect ratio of the tip apex may finally determine the feature size of the nanostructures. It is shown that the tips with higher curvature aspect ratios have advantages over those with lower aspect ratios in achieving smaller nanostructures.

From the STM images, it is found that the preprocessed substrate surfaces have a rms roughness of about 0.98 nm, while that derived from the AFM images was 0.6 nm. The difference in the roughness is due to the fact that the STM images result from the convolution of the surface topography and the local density of state (LDOS), while the AFM images only represent the surface topography.

Laser pulse energy, number of pulses, and tip-surface distance strongly affect the formation of the nanostructures as well as their geometries. By adjusting these parameters, nanostructures with different feature sizes (dot diameter or line width) and heights were fabricated. Figure 5 shows the STM images of the nanostructures fabricated using four different numbers of pulses (15, 10, 5, and 3) under the condition of 15 mJ pulse energy, 1 V gap voltage, and 3 nA tunneling current. In Figs. 5(a) and 5(b), two dots each were fabricated by 15 and 10 pulses, respectively. In Figs. 5(c) and 5(d), one dot each was fabricated by 5 and 3 pulses, respectively. It can be observed that these nanostructures have approximately circular shapes, due to the beam profile of the enhanced laser determined by the geometry of the tungsten tip. The brighter regions in the figures correspond to the regions which have higher electrical conductivity, or more precisely, higher tunneling probability. Therefore, the electronic properties of the fabricated structures are totally different from the silicon substrate. After analyzing the geometries of the nanostructures illustrated in Fig. 5, the pulse number dependence of the diameters and heights of the nanostructures was obtained and is shown in Fig. 6. It can be observed that the diameters and heights increase almost linearly with the increasing number of pulses. The diameters of the nanostructure range from 200 to 500 nm while their heights range from 4 to 16 nm.

In order to fabricate smaller nanostructures, more focused and enhanced optical field is required. According to the simulation results, this kind of optical field can be achieved by shorter tip-surface distance. In the experiments, this distance was controlled by tuning the gap voltage while keeping the same tunneling current. Different gap voltages (0.01, 0.1, and 1 V) combined with different pulse energies (2, 5, and 10 mJ) and a tunneling current of 3 nA were utilized to fabricate dots with the smallest possible diameters. A dot with a diameter of 30 nm, as illustrated in Fig. 7(a), was fabricated when the gap voltage and pulse energy were 0.1 V and 5 mJ, respectively. A single line, as shown in Fig. 7(b), was also fabricated by scanning the STM tip on the silicon surface. The tip scanning speed was 10 nm/s, and other conditions were the same as those used in the fabrication of the 30 nm dot. This line has an average width of approximately 30 nm.

STS provides vital information about the LDOS on surfaces at atomic or molecular scales.[31] H-passivated silicon surfaces show ideal surface electronic structure with a low surface state density.[32] The absence of surface states and Fermi level pinning enables direct observation of Schottky barrier behavior. The *I-V* curve of *p*-type silicon surfaces indicates a typical Schottky behavior, exponentially in the forward bias and lower current for reverse bias. As the substrate voltage is tuned more positive, the conduction band moves up and more current will flow. In the reverse direction, as the voltage becomes more negative, the bands bend down and increase the potential barrier to the holes.

STS was performed in different regions *in situ* after

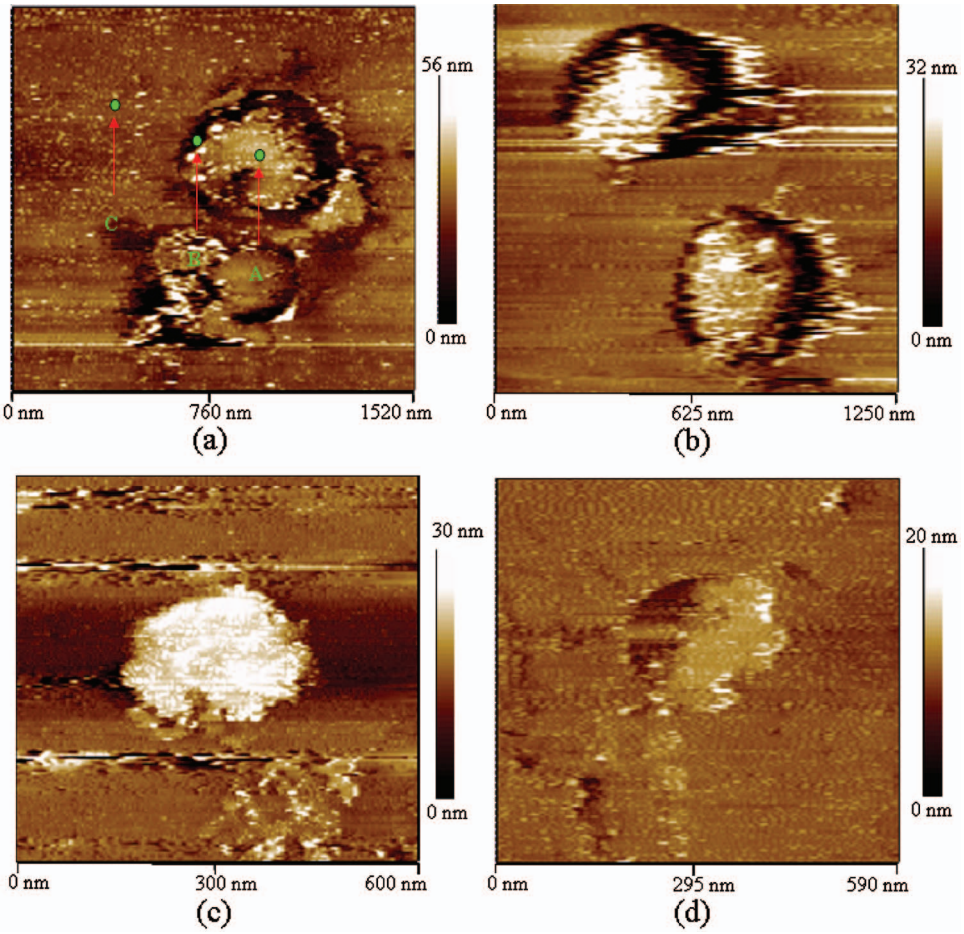

FIG. 5. (Color) STM images of the nanostructures fabricated with different pulse numbers of (a) 15, (b) 10, (c) 5, and (d) 3 (laser energy=15 mJ, gap voltage=1 V, tunneling current=3 nA).

nanostructuring. Tunneling currents as functions of the gap voltage at points A, B, and C indicated in Fig. 5(a) are shown in Fig. 8(a). It can be seen that the *I-V* characteristics are different in different regions. In the region far from the fabricated dot (curve C), a typical Schottky barrier behavior can be observed. At the edge of the dot (curve B), the tip-surface gap still demonstrates a Schottky behavior but with increased tunneling probability. Inside the dot (curve A), no obvious Schottky behavior can be seen. Furthermore, the curve becomes more symmetric and band bending disappears. The band gap can be estimated from the differential conductivity as a function of gap voltage, as shown in Fig. 8(b). For the H-passivated surface without laser processing, the band gap is around 1.1 eV, which is a typical value for silicon. The band gap of the silicon surface decreases when the probe point approaches the dot, and almost diminishes inside the dot, indicating the tendency of electronic structure change.

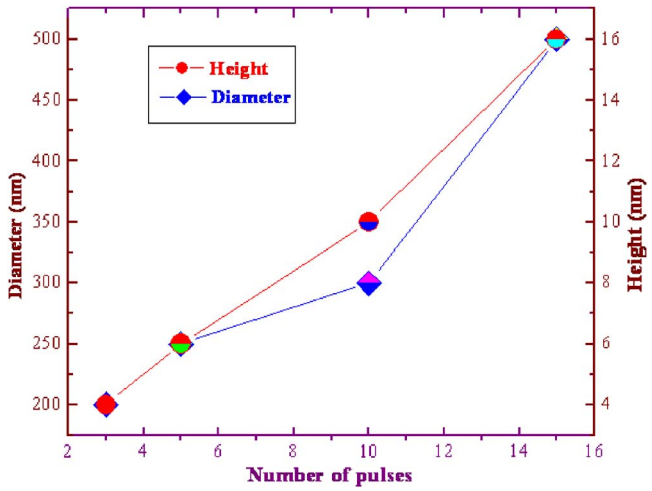

FIG. 6. (Color online) Pulse number dependence of the nanostructure diameter (diamonds) and height (circles) (pulse energy=15 mJ, gap voltage=1 V, tunneling current=3 nA).

The difference between the tip work function and the semiconductor electrode affinity results in the formation of a Schottky barrier. The conduction between the tip and the semiconductor surface involves thermionic emission of electrons over the barrier followed by tunneling of electrons through the vacuum barrier to the metal tip. An increasing positive sample bias on *p*-type silicon decrease the band banding, lowering the Schottky barrier and enhancing electron emission.[33] As illustrated by curves B and C in Fig. 8(a), these diodelike curves are a typical metal-insulator-semiconductor (MIS) tunneling. The spectra illustrate clearly the expected dependence on doping, meaning larger current in the positive sample bias as compared to that in the negative bias. The band bending can be concluded from the asymmetric behavior.

When the gap voltage is lower than both work functions of the tungsten tip and *p*-type silicon, the nanostructures with different differential conductance may arise from the surface states. These surface states are primarily associated with critical points in the surface-projected bulk band structures

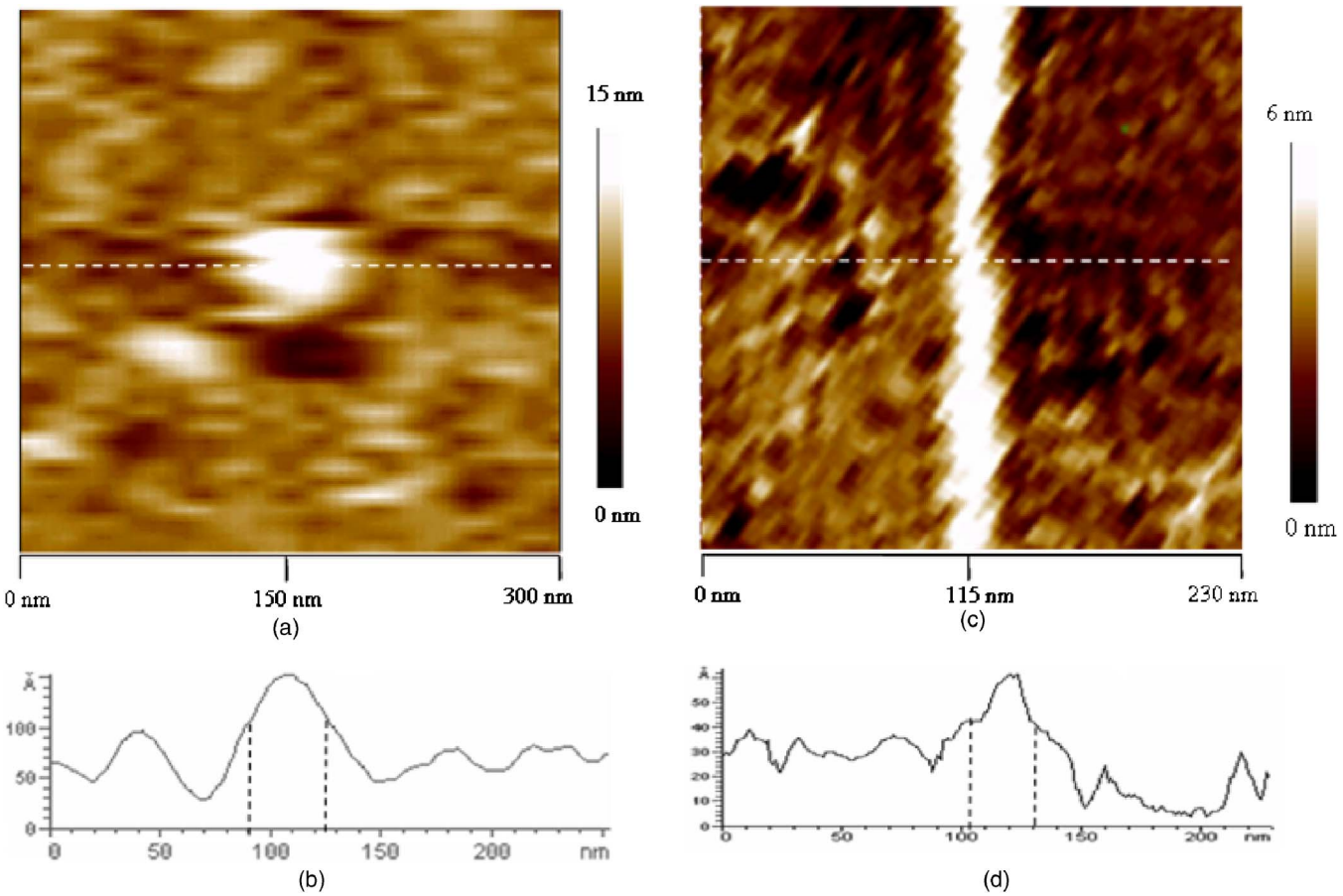

FIG. 7. (Color online) (a) STM image of a dot with a diameter of 30 nm, (b) profile along the line indicated in (a), (c) STM image of a line with a width of 30 nm, and (d) profile along the line indicated in (c) (gap voltage=0.1 V, tunneling current=3 nA).

or surface dangling bonds. The mechanisms of the nanostructure fabrication on the silicon surfaces by LA-STM might involve two individual steps: First, the hydrogen atoms adsorbed on the silicon surface for passivation are thermally desorbed by the highly localized optical field, resulting in a clean and intrinsic silicon surface. Second, the dehydrogenized surface is turned into more conductive poly-silicon through a thermal process. Therefore, the local temperature is of crucial importance in both steps. To better understand the mechanisms, a study of the temperature rise underneath the tip apex is necessary. It is assumed that the incident laser beam propagates in parallel with the sample surface. When a Gaussian distribution is used to describe the beam profile, the steady-state temperature on the silicon surface underneath the tungsten tip induced by a pulsed laser can be expressed by[13,34]

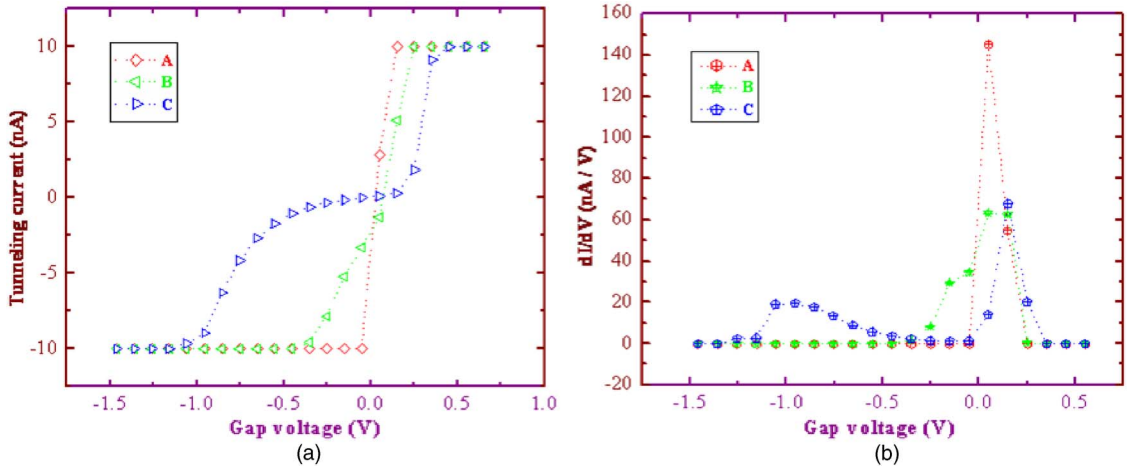

FIG. 8. (Color online) (a) *I-V* characteristics and (b) differential conductance dI/dV as a function of gap voltage at points A, B, and C indicated in Fig. 5(a).

$$T_{\max} = \frac{\sqrt{\pi}\alpha F(1-R_0)w_0}{8\kappa_T \tau}, \quad (5)$$

where $T_{\max}$ is the maximum temperature on the silicon surface underneath the tip apex, α is the optical enhancement factor defined as the ratio of the enhanced electric field to the original electric field of the incident pulsed laser, F is the laser fluence, R_0 is the optical reflectance of the silicon surface at the normal incidence,w_0 is the diameter of the tip apex, κ_T is the thermal conductivity of the silicon, and τ is the laser pulse duration. Obviously, the temperature induced by the LA-STM is proportional to the laser intensity F/τ, the optical enhancement factor, α, and the tip radius. Laser wavelength also affects the temperature because the optical reflectance is a function of the laser wavelength. Consequently, in order to increase the transient local temperature, we can use a pulsed laser with high peak energy and short pulse duration, or select a low gap voltage to maintain a short tip-surface distance that can lead to an increased optical enhancement factor, or employ a tip with a small tip radius. The temperature was calculated using parameters derived both from practical experimental conditions and simulation results: R_0 was 0.37 at 532 nm; α was 220 at a gap distance of 1 nm; w_0 was 30 nm for the EC-etched tungsten tip; κ_T was 1.3 W cm^{-1} $°C^{-1}$. For a pulsed laser with a pulse energy of 5 mJ and a pulse duration of 7 ns, the laser intensity F/τ was estimated as 30 mW cm^{-2}. As a result, the temperature is calculated to be 1259 °C, corresponding to the temperature at which the dot diameter of 30 nm was fabricated. This temperature is a slightly lower than the melting point of silicon (1412 °C). A threshold pulse energy to form a nanostructure was found to be 2 mJ. When using the same parameters given above, the threshold temperature was calculated to be 503 °C. When the temperature is under this threshold, either the photochemical reaction for dehydrogenization or the thermal process for the formation of polysilicon cannot undergo. Hence, no nanostructure can be fabricated on the silicon surface.

V. CONCLUSIONS

Nanoscale dots and lines with high electrical conductivity were fabricated on *p*-type silicon (110) substrate surfaces by LA-STM. The feature sizes and heights are nearly linearly dependent on the number of laser pulses. A dot with a diameter of 30 nm was fabricated with a pulse energy of 5 mJ, a gap voltage of 0.1 V, and a tunneling current of 3 nA. A line with a width of 30 nm was also fabricated with a tip scanning speed of 10 nm/s. STS spectra indicate that their electronic structures were changed. The nanostructures are presumably polysilicon, which has a higher electrical conductivity than that of the intrinsic silicon. Thermal effect induced by the enhanced optical field is used to explain the nanofabrication. The numerical simulation of the optical field underneath a tungsten tip shows that the optical field can more strongly be enhanced in presence of a silicon substrate. The enhancement is attributed to the lightning rod effects due to a geometrical singularity of a sharp tip.

ACKNOWLEDGMENTS

This work was financially supported by the National Science Foundation (CMMI 0457471 and ECCS 0619553) and Nebraska Research Initiative.

[1] Y. T. H. Togashi, A. Kato, A. Konno, H. Asaoka, and M. Suemitsu, Jpn. J. Appl. Phys., Part 1 **46**, 3239 (2007).
[2] N. Barniol, F. Perezmurano, and X. Aymerich, Appl. Phys. Lett. **61**, 462 (1992).
[3] J. A. Dagata, J. Schneir, H. H. Harary, C. J. Evans, M. T. Postek, and J. Bennett, Appl. Phys. Lett. **56**, 2001 (1990).
[4] A. A. Tseng, A. Notargiacomo, and T. P. Chen, J. Vac. Sci. Technol. B **23**, 877 (2005).
[5] P. M. Campbell, E. S. Snow, and P. J. McMarr, Surf. Sci. **362**, 870 (1996).
[6] K. Sattler, Jpn. J. Appl. Phys., Part 1 **42**, 4825 (2003).
[7] E. J. Vanloenen, D. Dijkkamp, A. J. Hoeven, J. M. Lenssinck, and J. Dieleman, J. Vac. Sci. Technol. A **8**, 574 (1990).
[8] S. Heike, T. Hashizume, and Y. Wada, J. Appl. Phys. **80**, 4182 (1996).
[9] J. Jersch and K. Dickmann, Appl. Phys. Lett. **68**, 868 (1996).
[10] Y. F. Lu, Z. H. Mai, G. Qiu, and W. K. Chim, Appl. Phys. Lett. **75**, 2359 (1999).
[11] Y. F. Lu, Z. H. Mai, W. D. Song, and W. K. Chim, Appl. Phys. A: Mater. Sci. Process. **70**, 403 (2000).
[12] Y. F. Lu, Z. H. Mai, Y. W. Zheng, and W. D. Song, Appl. Phys. Lett. **76**, 1200 (2000).
[13] Z. H. Mai, Y. F. Lu, W. D. Song, and W. K. Chim, Appl. Surf. Sci. **154**, 360 (2000).
[14] X. W. Wang, J. Phys. D **38**, 1805 (2005).
[15] X. W. Wang and Y. F. Lu, J. Appl. Phys. **98** (2005).
[16] V. A. Ukraintsev and J. T. Yates, J. Appl. Phys. **80**, 2561 (1996).
[17] Z. Dohnalek, I. Lyubinetsky, and J. T. Yates, J. Vac. Sci. Technol. A **15**, 1488 (1997).
[18] W. X. Sun and Z. X. Shen, Ultramicroscopy **94**, 237 (2003).
[19] L. Gomez, R. Bachelot, A. Bouhelier, G. P. Wiederrecht, S. H. Chang, S. K. Gray, F. Hua, S. Jeon, J. A. Rogers, M. E. Castro, S. Blaize, I. Stefanon, G. Lerondel, and P. Royer, J. Opt. Soc. Am. B **23**, 823 (2006).
[20] F. Demming, J. Jersch, K. Dickmann, and P. I. Geshev, Appl. Phys. B: Lasers Opt. **66**, 593 (1998).
[21] A. Hartschuh, M. R. Beversluis, A. Bouhelier, and L. Novotny, Philos. Trans. R. Soc. London, Ser. A **362**, 807 (2004).
[22] E. Hartmann, R. J. Behm, G. Krotz, G. Muller, and F. Koch, Appl. Phys. Lett. **59**, 2136 (1991).
[23] H. A. Lin, R. Jaccodine, and M. S. Freund, Appl. Phys. Lett. **72**, 1993 (1998).
[24] R. M. Ostrom, D. M. Tanenbaum, and A. Gallagher, Appl. Phys. Lett. **61**, 925 (1992).
[25] S. T. Yau, X. Zheng, and M. H. Nayfeh, Appl. Phys. Lett. **59**, 2457 (1991).
[26] K. J. Yi, H. Wang, Y. F. Lu, and Z. Y. Yang, J. Appl. Phys. **101** (2007).
[27] M. I. Markovic and A. D. Rakic, Opt. Laser Technol. **22**, 394 (1990).
[28] M. I. Markovic and A. D. Rakic, Appl. Opt. **29**, 3479 (1990).
[29] A. Bouhelier, Microsc. Res. Tech. **69**, 563 (2006).
[30] A. Bouhelier, M. R. Beversluis, and L. Novotny, Abstr. Pap. - Am. Chem. Soc. **227**, 250 (2004).
[31] R. J. Hamers, Annu. Rev. Phys. Chem. **40**, 531 (1989).
[32] W. J. Kaiser, L. D. Bell, M. H. Hecht, and F. J. Grunthaner, J. Vac. Sci. Technol. A **6**, 519 (1988).
[33] P. E. W. J. Jahanmir, A. Young, and T. N. Rhodin, J. Vac. Sci. Technol. A **7**, 2741 (1989).
[34] D. J. Ehrlich and J. Y. Tsao, in *Laser Microfabrication—Thin Film Processes and Lithography* (Academic, San Diego, 1989), p. 268.